



## Thermal Performance Optimization of Helically Baffled Conical Cavity Receivers for Solar Dish Concentrators

Sarmad S.A. Talib\*<sup>ID</sup>, Ra'ad K. Mohammed Al Dulaimi<sup>ID</sup>

Department of Mechanical Engineering, Al-Nahrain University, Baghdad 10001, Iraq

Corresponding Author Email: [sarmdsalam@gmail.com](mailto:sarmdsalam@gmail.com)

Copyright: ©2024 The authors. This article is published by IIETA and is licensed under the CC BY 4.0 license (<http://creativecommons.org/licenses/by/4.0/>).

<https://doi.org/10.18280/ijht.420529>

### ABSTRACT

**Received:** 21 July 2024

**Revised:** 13 September 2024

**Accepted:** 19 September 2024

**Available online:** 31 October 2024

#### Keywords:

*conical cavity, solar dish, thermal performance optimization, CFD, pressure drop, thermal analysis*

Cavity receivers are crucial components of solar dish concentrators, as their design significantly influences thermal efficiency. This paper presents an optimized design for conical cavity receivers incorporating helically baffled paths to enhance thermal performance. Through computational fluid dynamics (CFD) simulations, three groups of models were studied to maximize outlet temperature and minimize pressure drop. Group A conducted a parametric study on key design variables, including conical length, baffle pitch, and inclination. Group B introduced fined paths based on the optimal configuration from Group A, while Group C further refined these designs with multi-staged helically baffled paths. The optimized design achieved a peak outlet temperature of 301.97 K and a minimal pressure drop of 145.835 Pa at a water flow rate of 2 L/min. These results demonstrate the potential of helically baffled conical cavity receivers to significantly improve the thermal efficiency of solar dish concentrators, offering a novel contribution to the field of solar thermal energy systems.

## 1. INTRODUCTION

With growing global demand for sustainable and clean energy sources, solar energy moves to the frontline of promising solutions for meeting this demand while mitigating adverse environmental impacts associated with traditional energy sources [1, 2]. Solar energy has been used in many technologies such as: heating water and air [3, 4], desalination [5, 6], cooking food [7, 8], generating electricity [9, 10], etc. Of all the several solar technologies, solar dish concentrators best harness solar energy by concentrating it on a receiver, thereby exponentially increasing the efficiency of any solar power system [11, 12]. At the same time, despite considerable progress in solar dish concentrator technology, some challenges exist in minimizing thermal losses and increasing the efficiency of heat absorption [13].

It implies that the performance of the receiver dictates, to a great extent, overall performance and efficiency of a solar dish concentrator. For this reason, traditional designs of receivers frequently have poor efficiency due to non-optimal heat transfer and larger thermal losses, resulting in overall poor system performance. These challenges further raise the need to explore new designs of receivers that can handle these issues in a better way [14].

It focuses on the design of the receiver, with a novel approach involving a conical cavity receiver with helical baffles. It is introduced that helical baffles will increase the heat transfer in a cavity by increasing the turbulence of the flow, hence reducing thermal losses and improving the overall thermal efficiency of the system. Such theoretical benefits need to be checked by a proper thermal analysis for the design

developed, leading to the main parameters that have an effect on the performance of the receiver.

This research will primarily focus on the assessment of the thermal performance of the helically baffled conical cavity receiver, comparing its efficiency with conventional designs of receivers, and identifying what factors mostly influence its thermal behavior. These objectives are pursued through the following structure of the study: first, the literature review presents a solid background of existing designs for receivers and explains the limitations; second, the methodology describes the experimental setup and analysis techniques used in this study; third, the results present the findings on thermal analysis; and lastly, the discussion and conclusion sections that follow interpret these results and outline their implications for future research and practical applications in solar energy technologies.

The gap in the current research lies in the lack of empirical validation and optimization of conical cavity receivers with helically baffled designs. While theoretical studies suggest that helical baffles can enhance heat transfer and reduce thermal losses, there is limited experimental evidence and detailed thermal analysis on their performance compared to conventional receiver designs. This research aims to address these gaps by optimizing key design parameters and providing a comprehensive thermal performance evaluation of helically baffled conical cavity receivers.

It proposes and analyzes a novel receiver design with potential to significantly improve the thermal performance of solar dish systems, thereby contributing to the development of more efficient solar concentrators.

## 2. CONICAL CAVITIES RECEIVERS REVIEW

Lately, conical-cavity receivers have raised interest in solar dish concentrator technology, due to some of their special properties: improvement in thermal efficiency and minimization of heat dissipation. The geometrical additions in a conical cavity receiver, unlike a typical receiver design, involve helically formed absorber tubes with disturbances flat back plates and cone frustums that are aimed uniquely at the improvement of heat transfer and making temperatures distributed more uniformly.

### 2.1 Thermodynamical researches on conical cavity receivers

Pavlovic et al. [15] performed a very detailed simulation study where the researchers compared the thermal efficiencies of conical and spiral cavities in solar receivers. According to their results, at an oil input temperature of 200°C, the highest thermal efficiency achieved by the conical cavities was as high as 78.7%, much higher than that of the spiral cavities with 56.0%. This was because the optical efficiency of the conical cavity was greater by a difference of 1.15%.

Pavlovic et al. [16] evaluated the exergy and energy efficiencies of conical cavity receivers for three working fluids: water, air, and Therminol VP1. Their results showed the highest possible exergy efficiency was obtained using the Therminol VP1 fluid at 155°C inlet temperature, which was 8%. At low temperature ranges, the highest possible thermal efficiency was attained with water, while at higher temperature values, the best was obtained with Therminol VP1.

A study by Li et al. [14] has been done on the design of a conical cavity receiver featuring a spiral tube with Therminol VP1 as the working fluid. The results showed that a temperature difference of 81 K between the inlet temperature

and the ambient temperature could produce a thermal efficiency of 60%.

### 2.2 Experimental research on conical cavity receivers

Thirunavukkarasu et al. [17] conducted experimental studies on the energy and exergy performance of conical cavity receivers. Their results indicated that for a flow rate of 2.5 L/min, the maximum thermal efficiency reached was approximately 66.75% and the efficiency in exergy was 10.35%. Key to these results was the position of the receiver tube inside the cavity.

Chu et al. [18] performed an experiment on a pressurized air receiver that was fitted with dual spiral tubes within a conical chamber. They demonstrated a thermal efficiency of 53.16% and a power of 3.96 kW at a flow rate of 0.0048 kg/sec. In related work, for the same system but with an exterior spiral tube configuration, they showed efficiencies of 56.21% thermal and 5.45% exergy.

Venkatachalam and Cheralathan [19] studied the effects of L/D on the conical cavity receiver's thermal performance. Their findings reported an increase in temperature and thermal performance of the receiver with a decrease in aspect ratio. The optimum aspect ratio was 0.80, for which it returned a minimum heat loss of 58 W/K.

### 2.3 Design and modeling on conical cavity receivers

Purpose: Bashir and Giovannelli [20] combined PCM in designing another scheme to increase the performance of some conical cavity receivers. An optimum distribution of temperature of PCM and along a cavity wall temperature was achieved by this 30 cm long conical cavity with 21 cm diameter at its opening middle [21].

**Table 1.** A summary of the conical cavity receiver reviews

Ref.	Study Type	Brief Title	Highlights
Pavlovic et al. [15]	Simulation	Cavities Operation	For the spiral and conical cavities, maximum optical efficiencies were approximately 84.06% and 85.21%, respectively.
Pavlovic et al. [16]	Both Experimental and Numerical	Cavity's Thermal Efficiency	The best exergy and thermal efficiencies have been obtained by using a working fluid of Therminol VP-1, which was equal to 8% and 34%, respectively.
Li et al. [14]	Simulation	Conical Operation Using a Spiral Tube	At a flow rate of 0.5L/s and an ambient/inlet temperature differential of 81 K, 60% thermal efficiency was achieved.
Thirunavukkarasu et al. [17]	Experimental	Performance of Conical Frustum Cavity	At a flow rate of 2.5 L/min, the maximum thermal efficiency and energy were around 66.75% and 10.35%, respectively.
Chu et al. [18]	Experimental	Thermal Exam of the Cavity	The thermal efficiency and power production with two spiral tubes and a 4 mm inner diameter tube have been 53.16% and 3.96KW, respectively.
Venkatachalam and Cheralathan [19]	Experimental	Aspect Ratio's Impact on Efficiency	The overall heat loss factor decreased to 58 W/K by an aspect ratio of 0.8.
Bashir and Giovannelli [20]	Numerical	Thermal Retention of Energy	Si-Mg was used as PCM, and because of its great heat conductivity, PCM has been completely melted with a constant temperature distribution.
Hernandez et al. [22]	Both Experimental and Simulation	Effective Cavity Performance Parameters	The cavity efficiency rose when flow rate was increased, and inlet temperature was lowered.
Xiao et al. [23]	Simulation	Maximum Recipient Efficiency	With 8 loops and a cavity angle of 150, the optimal optical efficiency was attained.
Zhang et al. [24]	Both Numerical and Simulation	Cavity Performance Study	An ideal cavity inclination angle of 50 produced an overall efficiency of 63.6%.

Khalil et al. [21] tried to prevent overheating of the cavity receiver surface by introducing an Inconel spot-welded variable shape. Hernandez et al. [22] used a dish concentrator with a 90° rim angle with a conical cavity receiver. They found out that by increasing the diameter of the inner side of the cavity, the concentration value increased, and that increasing the outer side of the cavity was the opposite.

There are also reports on simulation studies that inquired into the optical efficiency of different conical cavity geometries with varying numbers of tube loops and inclination. For example, Xiao et al. [23] reported that optimum results were obtained with eight loops tilted at an inclination of 15°. It was observed from the results that while increasing the number of loops, thermal and overall efficiency increased; however, with further inclination, efficiency declined.

These studies collectively highlight the potential of conical cavity receivers to significantly enhance the thermal performance of solar dish concentrators. However, the ongoing challenges related to optimizing heat transfer and minimizing thermal losses underscore the need for continued research and innovation in this area. A few key details regarding the conical cavity receivers are shown in Table 1.

### 3. THE PRESENT WORK

The literature review indicates a significant interest in enhancing the design of conical cavity receivers for solar dish concentrators, driven by the necessity for creating highly efficient systems. The primary motivation for this research is the persistent need to optimize thermal performance while minimizing energy losses. In this context, the present study introduces and examines a novel design for conical cavity receivers, incorporating helically baffled structures. These baffles are designed to increase thermal efficiency and reduce pressure losses within the receiver.

The study explores a wide range of configurations and sizes for helically baffled conical cavity receivers to identify the optimal shape and configuration. The optimization process focuses on maximizing thermal efficiency and minimizing pressure drops, with all designs evaluated using these two objective functions. To our knowledge, this study represents one of the most comprehensive comparative analyses of conical cavity receivers, integrating optical, thermal, and exergy considerations under various operating conditions. Previous literature has often limited the optimization of cavity receivers to optical performance alone, which does not always translate to the highest thermal efficiency or maximum useful heat production.

This research employs advanced Computational Fluid Dynamics (CFD) simulations to conduct a detailed parametric analysis of the proposed receiver designs. Additionally, the study includes experimental validation to confirm the accuracy of the CFD results and ensure their applicability in real-world scenarios.

#### 3.1 CFD modeling

This section describes the methodology used in this research—Computational Fluid Dynamics. CFD was found very convenient for this research project because it is adaptable to a wide range of geometries and boundary conditions, important in developing and enhancing the design

of cavity receivers. Recent improvements in numerical modeling have improved the credibility and accuracy of CFD; hence, making the technique valuable in conducting detailed parametric analyses in advance of physical testing. This has the possibility of great time reductions and cost savings in the development of new designs for receivers.

The CFD methodology employed in this study includes the following steps:

1. **Model Creation and Setup:** The receiver models were created using SolidWorks and imported into Ansys for CFD simulation. The models included two main domains: the receiver body and the fluid domain. The outer surface of the fluid domain was fully insulated, while the internal surface of the copper metal receiver was exposed to a uniform heat flux.
2. **Boundary Conditions:** The boundary conditions were carefully selected to replicate realistic operating conditions. These included a heat flux of 3000 W/m<sup>2</sup>, reflecting the highest solar irradiation levels typically observed in the Iraqi region. The inlet water temperature was set at 24°C, and the water flow rates were varied between 2, 3, and 4 L/min to assess the impact of flow rate on thermal performance and pressure drop.
3. **Mesh Generation:** A high-quality mesh was generated for each model, ensuring sufficient resolution in areas with high gradients in temperature and velocity. The mesh independence was tested to ensure that the results were not influenced by the mesh size, allowing for accurate and reliable simulation outcomes.
4. **Validation:** The CFD results were validated against experimental data to confirm their accuracy. This validation process is crucial for ensuring that the CFD predictions are reflective of real-world performance and can be reliably used to guide the design and optimization of conical cavity receivers.
5. **Parametric Analysis:** The simulations were used to conduct a detailed parametric analysis, exploring the impact of various design parameters such as conical length, baffle pitch, baffle height, conical inclination, and upper conical diameter on thermal performance and pressure drop. This analysis provided insights into the optimal design configurations that maximize thermal efficiency while minimizing pressure losses.

Overall, the CFD methodology employed in this study provided a robust framework for optimizing the design of helically baffled conical cavity receivers, with the results offering valuable insights for enhancing the thermal efficiency of solar dish concentrators. The combination of advanced numerical modeling and experimental validation ensures that the findings are both accurate and applicable in practical solar energy systems.

#### 3.2 Computational domains

The computation domain represents the geometries that specify the shape and size of the computation interest region. The models were created by using SolidWorks software and then imported to Ansys. There is two modeled domines, receiver body and the fluid. The outer surface of the fluid domain is completely insulated, Whereas the internal side of the copper metal is exposed to heat flux. All surfaces are assumed to be smooth. The physical and computational domains are shown in Figure 1.



**Figure 1.** A solar dish system, the physical and CFD domains

### 3.3 The examined cavity receivers

In this work, three different conical cavity receiver's groups are investigated. Every group consists of a several shape configurations to nominate the optimal design using the thermal efficiency maximization criterion and then the optimum cases are compared. The examined designs groups of the cavity receivers have the following shapes configurations: Group A (helically baffled path), Group B (helically baffled fined path), Group C (multi stages helically baffled fined path). Figure 2 illustrates the helically baffled path, where Figures 3 and 4 show the heliacally baffled fined path. Were, Figure 5 shows the multistage helically baffled fined path. Group A (the helically baffled path) tested the conical cavity receiver variables such as the optimal length of the conical, the optimal baffle pitch distance and height, the optimal conical inclination, or the upper conic diameter). Were the aperture of the conical receiver is fixed with 270 mm.

Depending on the Fixed Aperture of the Conical  $D=270$  mm, the other variables made as a relation with it, the length started with  $L=0.5D$ ,  $L=1D$ ,  $L=1.5D$ . Whereas the upper helical diameter ( $d$ ) ranged from  $d=0.1D$ ,  $d=0.2D$ ,  $d=0.3D$ . The  $d$  changes typically change the inclination angle if the conic. The helically baffle pitch ( $P$ ) is an important variable which effect on the thermal efficiency and pressure drop. the Baffle pitch was tested with the sizes (10 mm, 15 mm, 20 mm) Table 2 specifies the Group (A) variable.

**Table 2.** Group (A) the helically baffled path parameters

Receiver Aperture Diameter	D	270 mm
Receiver Upper Diameter	d	27, 54, 81 mm
Conical Length	L	135, 270, 405mm
Baffle Pitch	p	10, 15 ,20 mm

**Table 3.** Group (B) helically baffled fined path parameters

Receiver Aperture Diameter	D	270 mm
Receiver Upper Diameter	d	81 mm
Conical Length	L	405 mm
Baffle Pitch	p	25, 40, 60 mm
Fin Size	f	3, 6, 9 mm

The Group (B) (the helically baffle fined path) tested a new concept of the conical cavity receiver, this concept was achieved by changing the way of the fluid flow, in the conventional conical cavity receivers the fluid flows in closed

helically path through a circular tube in the helically baffle fined path the flow of fluid is from the bottom to the top through an annular fluid inlet, the fined baffles mix and circulate the fluid, causing an increasing in thermal efficiency and reducing in pressure losses as illustrated in path Figure 4.

Group (B) depended on the results of Group (A) to fix some variables in group A to reduce the tested cases, where the inclination angle (the upper diameter  $d$ ) and the conical length is fixed in Group (B). Also, like the other groups, the aperture diameter is also constant. Table 3 illustrates the Group (B) parameters.

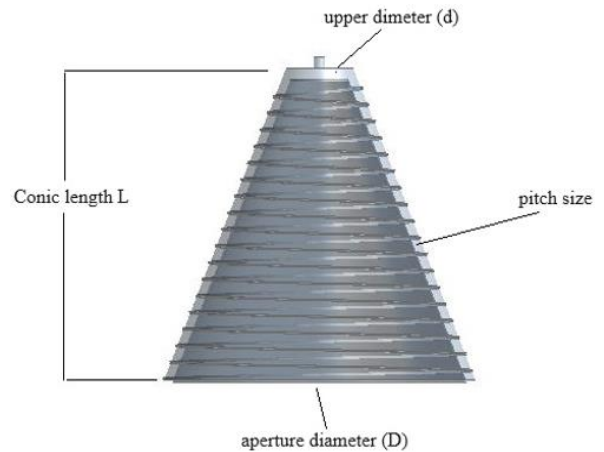


**Figure 2.** The helically baffled conical cavity receiver

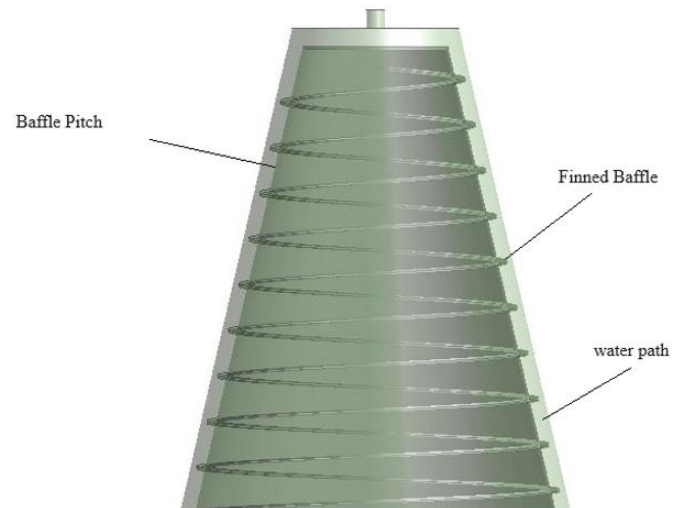


**Figure 3.** The helically baffled fined path conical cavity receiver

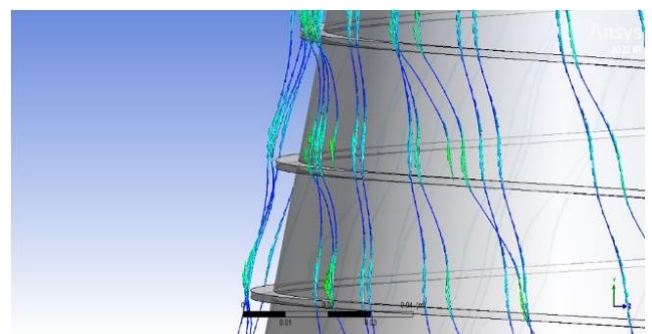


**Figure 4.** The helically baffled fined path conical cavity receiver flow stream direction

Due to the promised results from Group (B), Group (C) (multi stages helically baffled fined path) comes as a feature to enhance in thermal efficiency of Group (B). Figure 5 shows the multi stages helically baffled fined path. As illustrated in Table 4, the multi stages helical baffled fined path used a two helical baffled fin with different size. One of them is 3 mm and the other is 6 mm. this will enhance the fluid mixing inside the receiver leading to an enhancement in the thermal efficiency.

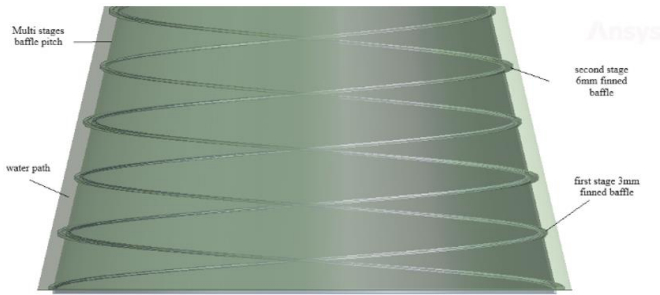


Figure 5. Multi stages helically baffled fined path

Table 4. Group (C) helically baffled fined path parameters

Receiver Aperture Diameter	D	270 mm
Receiver Upper Diameter	d	81 mm
Conical Length	L	405 mm
Baffle Pitch	p	30, 60, 90 mm
Multiple Fins Size	f	3 and 6 mm together

### 3.4 Basic considerations and boundary conditions

The proper boundary conditions are selected to study the problem precisely. According to the area of the solar dish aperture area 3 m<sup>2</sup>, the selected heat flux is 3000 W/m<sup>2</sup>, those will match the highest solar irradiation in Iraqi region. Below, the boundary conditions list and it is illustrated in Figure 6.

- The internal surface exposed a heat flux of 3000 W/m<sup>2</sup>.
- External surface is totally insulated.
- The inlet water temperature is 24°C in all cases.
- The Outlet water pressure is 0 pa.
- Zero incident angle because the solar dish follows the sun in two directions.
- The mass flow rate (*m*) is selected at 2,3,4 l/m.

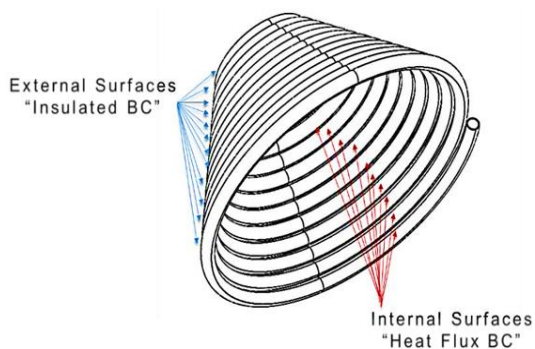


Figure 6. Boundary conditions for CFD simulations

In all investigated cases, Water is used as a working fluid. Below are the physical assumptions considered to solve heat and fluid flow features are:

- Working fluid (Water) is a Newtonian fluid in which viscous stresses are linearly proportioning to the local strain rate.

- Water is an incompressible continuous substance. Thus, the fluid particle and the details of the structure of the molecules are ignored.
- No phase change occurs during the study.
- Water properties varied with the temperature only.
- Heat losses on the cavity surfaces are subtracted from the concentrated absorbed flux.
- No heat generation within the solid domain.
- Chemical reaction and compression work are negligible.
- Gravity force is embedded.

### 3.5 Governing equations and turbulence modeling

Since the working fluid is assumed to be Newtonian, the Navier-Stokes equation can describe the fluid flow. Hence, the heat transfer and fluid flow under discussion are governed by the Navier-Stokes equation and the energy transport equation. The primary equations that govern the system are typically continuity, Navier-Stokes (momentum), and energy equations, all expressed in differential form. The equation of continuity, which is derived from the laws of mass conservation, is commonly useful when considering the assumptions of incompressible fluid flow [25, 26].

$$\nabla \cdot V = 0 \quad (1)$$

The Navier-Stokes equation is a fundamental representation of fluid flow, derived from momentum theory and presented as follows [25].

$$\rho \frac{DV}{Dt} = -\nabla p + \rho g + \nabla \cdot \mu(\nabla V) \quad (2)$$

Energy equation obtained from energy conservation principles. While fluid crossing the boundary, it will carry its internal thermal, kinetic, and potential energy. The potential energy is neglected for the sake of brevity. The energy equation under these conditions takes the following form [25, 27].

$$\rho c_p \left( \frac{\partial T}{\partial t} + \nabla \cdot VT \right) = \nabla \cdot (k \cdot \nabla T) \quad (3)$$

The thermal conductivity is mentioned as (*k*) and (*c<sub>p</sub>*) is the heat capacity at constant pressure. However, the general governing Eqs. (1) to (3) apply to the laminar regime. In turbulent flow, a rise of fluctuating temperature and velocities in the governing equations should have appeared. Therefore, predictions of turbulent characteristics can be based on the time-average properties of turbulence. To achieve this, it is needed to employ the Reynolds Averaged Navier-Stokes (RANS) equations.

In RANS averaging, the instantaneous solution variables  $\varphi(\mathbf{V}, p, T)$  in the Navier Stokes equations are decomposed into mean  $\bar{\varphi}(\bar{u}, \bar{p}, \bar{T})$  and fluctuating components  $\hat{\varphi}(\hat{V}, \hat{p}, \hat{T})$ , mathematically written as:

$$\varphi = \bar{\varphi} + \hat{\varphi} \quad (4)$$

Then time averaging operations should be applied to Eq. (4) to produce a term as  $(\bar{\varphi} + \hat{\varphi} = \bar{\varphi})$ , where ( $\hat{\varphi} = 0$ ). Thus, by applying these to the momentum equation, the time-averaged

Navier-Stokes equation can be written in the form [25, 28]:

$$\rho \frac{Du_i}{Dt} = -\frac{\partial p}{\partial x_1} + \frac{\partial}{\partial x_i} \left( \mu \frac{\partial u_i}{\partial x_i} - \overline{\rho u_i u_j} \right) + S_i \quad (5)$$

where,  $(S_i)$  represents the gravitational term and  $(-\overline{\rho u_i u_j})$  is known as the Reynolds stresses, which are defined partially by the Boussinesq approach [25, 28]:

$$-\overline{u_i u_j} = \nu_t \left( \frac{\partial u_i}{\partial x_j} + \frac{\partial u_j}{\partial x_i} \right) - \frac{2}{3} \mathbf{k} \delta_{ij} \quad (6)$$

where,  $(\nu_t)$  is the turbulent kinematic viscosity,  $(\mathbf{k})$  the turbulent kinetic energy and  $(\delta_{ij})$  is called Kronecker delta, which is a function of two variables, usually just positive integers. The function has a value of (1) if the variables are equal and (0) otherwise. In the same way, as in Eq. (5), the time-averaged energy equation is [25].

$$\frac{\partial}{\partial x_i} (u_i T) = \frac{\partial}{\partial x_i} \left( \frac{k_{eff}}{\rho c_p} \frac{\partial T}{\partial x_j} - \overline{u_j T} \right) + S_i \quad (7)$$

where,

**Table 5.** Mesh independence procedure for helically baffled conical cavity and  $T_{in} = 24^\circ\text{C}$

Number of Elements	1,171,746	2,129,014	3,643,568	4,850,645	5,802,901	6,581,728
$T_{out}$ ( $^\circ\text{C}$ )	27.6	27.8	27.9	28	28.1	28
$\eta_{th}$	66.8%	67%	67%	67.1%	67.2%	67.1%
$f_r$	0.71	0.14	0.08	0.05	0.04	0.04

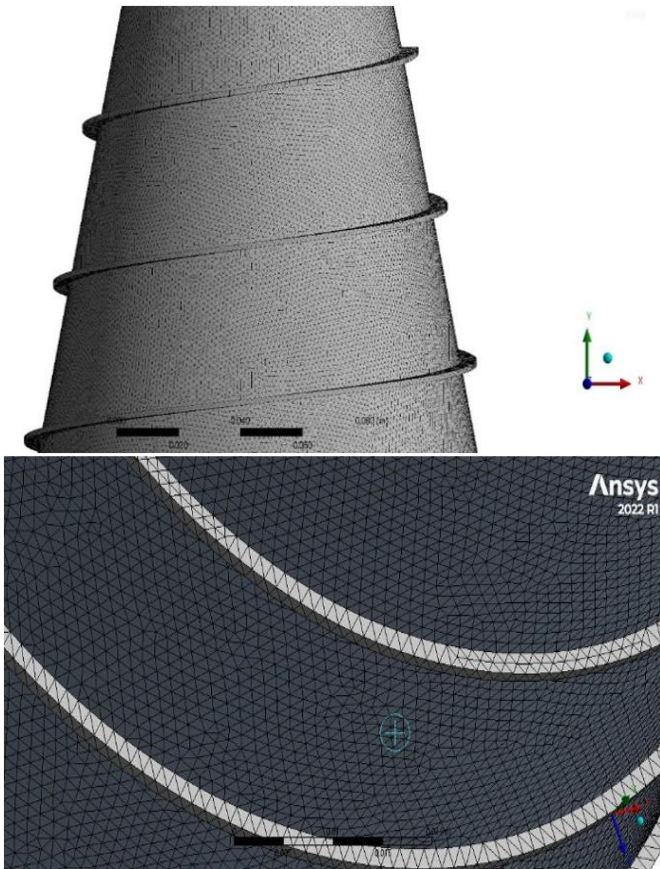


**Figure 7.** Generated mesh

$$\overline{u_j T} = -\frac{\nu_t}{\sigma_t} \frac{\partial \tau}{\partial x_j} \quad (8)$$

$(\sigma_t)$  is the turbulent Prandtl number. It's clear that these last governing equations have additional unknown variables such as turbulent viscosity. Many turbulent models are created to determine these variables as known quantities. The common models are Standard, RNG, and Realizable  $k-\epsilon$  models and Standard and SST  $k-\epsilon$  models. In our modeling we use  $k-\epsilon$  models, thus depended on a similar works which shows that the  $k-\epsilon$  models give results that are more similar to the experimental results.

### 3.6 Mesh configuration

The Tetrahedron mesh is selected in our simulation. A mesh independency procedure is followed and the results are given in Table 5. The final mesh consists of around 5.8 million elements. Special attention has been given to the fluid cells, ensuring a denser mesh distribution within the fluid regions and the partial cells to optimize accuracy. This procedure is performed for the for helically baffled conical cavity and for inlet temperature equal to  $24^\circ\text{C}$ . Figure 7 shows the generated mesh, and Figure 8 shows the mesh generated from some cases.

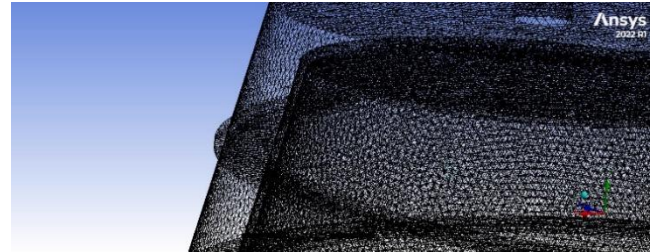


**Figure 8.** The generated mesh in the helically baffled cavity receiver

### 3.7 Mathematical formulation

This section presents the fundamental equations used for assessing the performance of the solar collector. The incident solar energy on the collector's aperture ( $Q_s$ ) is determined by multiplying the aperture area of the dish ( $A_a$ ) by the direct solar beam radiation ( $G_b$ ).

$$Q_s = A_a \cdot G_b \quad (9)$$

The useful heat production ( $Q_0$ ) is calculated as below:

$$Q_u = m \cdot c_p \cdot (T_{out} - T_{in}) \quad (10)$$

The thermal efficiency ( $\eta_{th}$ ) is calculated as below:

$$\eta_{th} = \frac{Q_u}{Q_s} \quad (11)$$

The heat transfer coefficient ( $h$ ) is measured as in this equation:

$$h = \frac{Q_u}{A_{coil} \cdot (T_{rec} - T_{fm})} \quad (12)$$

The mean fluid temperature ( $T_{fm}$ ) is calculated as:

$$T_{fm} = \frac{T_{in} + T_{out}}{2} \quad (13)$$

Nusselt number has always been an important parameter in evaluating the performance of most thermal applications [29, 30]. The Nusselt number ( $Nu$ ) is calculated by using the following equation:

$$Nu = \frac{h \cdot D_{coil,in}}{k} \quad (14)$$

The Reynolds number parameter is important for describing the flow behavior both for this application and other related applications such as heat exchangers [31, 32]. The Reynolds number ( $Re$ ) for the tubular coil is calculated as:

$$Re = \frac{\rho v D_h}{\mu} \quad (15)$$

The EEC was determined to assess the capacity to absorb solar energy and was linked to the works of Moshab and

Aldulaimi [33], Ma et al. [34], and Webb [35]. This formula was employed to compare the helically baffled finned cavity receiver model with the base model (circular receiver) under identical operating conditions and with the same power usage for pumping. A higher thermal improvement index (EEC) corresponds to a greater thermal performance. The EEC is a common standard used to assess the different configurations of heat exchangers.

$$EEC = \frac{Q/Q_o}{\Delta P/\Delta P_o} \quad (16)$$

where,  $Q_o$  and  $\Delta P_o$  represent the  $Q$  and  $\Delta P$  of the base model (circular receiver).

## 4. EXPERIMENTAL WORKS

### 4.1 Receiver model manufacturing

From the CFD results we found that, best results obtained from the helically baffled finned path. Where the optimal specification was with the 3 mm finned baffle. For CFD validation purposes the optimal receiver was manufactured and experimentally tested during peak time. The model is manufactured totally from pure copper with 0.6 mm thickness. Figure 9 illustrates the manufactured helically baffled finned conical cavity receiver. Also, a circular solar receiver designed by CFD and manufactured to work as a reference to our tests. Figure 10 shows the circular receiver.



a. The internal finned baffled path



b. The external shape of the cavity receiver

**Figure 9.** The manufactured helically baffled finned conical cavity receiver

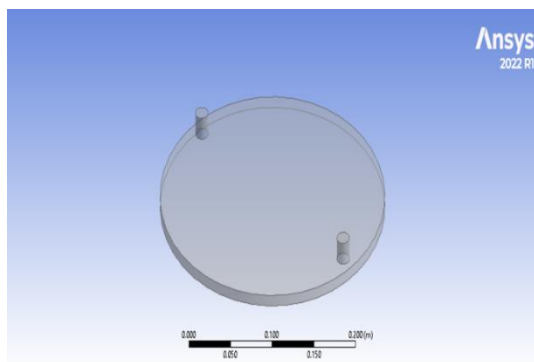


**Figure 10.** The reference circular solar receiver

## 4.2 Solar dish concentrator SDC manufacturing

The main reflective frame is composed of 24 ribs, each crafted from 6 mm steel plates, which were cut into parabolic curves and then covered with a highly reflective sheet. These ribs are attached to five ring strips, also made of 6 mm steel plates, to form the complete structure. The solar dish concentrator (SDC) is mounted on an iron support leg with a height of 110 cm. The collector is capable of rotating around two axes using linear actuators: one along the north-south axis and the other along the west-east axis. This allows the collector's aperture to be continuously oriented from sunrise to sunset throughout the year. Figure 11 illustrates the SDC structure, while Table 6 details its characteristics.

Table 6. The SDC characteristics

Feature	Value	Feature	Value
Aperture area, $A_a$	3.04 m <sup>2</sup>	Material of the tubes	Copper
Concentrator outer diameter	2 m	Rim angle, $\psi_r$	45.24
Concentrator inner diameter	0.36 m	Working fluid	Water
Collector depth, $C_d$	208 mm	Concentration ratio, $C_o$	38
Focal length, $f$	1200 mm	Direct solar radiation, $I_d$	910.47



Figure 11. The manufactured SDC structure

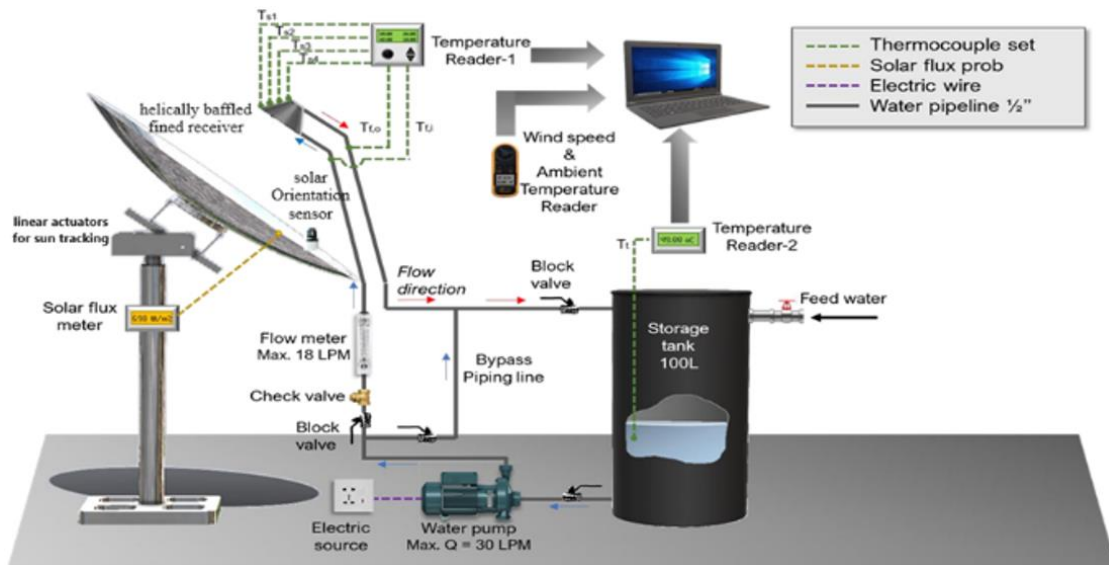


Figure 12. A schematic of the experimental system of SDC

## 4.3 Experimental setup and test procedure

A sketch of the experimental system and a photograph of the SDC are shown in Figure 12.

The studies began in May and were conducted daily from 7 AM to 6 PM. First, the water circulation pump was turned on, and the water flow rate was carefully regulated using a bypass mechanism. This configuration guaranteed ideal circumstances for the solar tracking system, which was fueled by the generated electricity. The data gathering process was conducted with great attention to detail, utilizing a data logger and strategically placed sensors on the solar receiver to accurately capture values. Figure 13 shows the experimental SDC system.



Figure 13. The experimental system of SDC

## 5. RESULTS AND DISCUSSION

This section investigates the effects of shape variations in the helically baffled conical cavity receiver on thermal performance and pressure losses. The analysis focuses on how the receiver height, inclination angle, baffle pitch size, and baffle configuration impact these performance metrics. Additionally, the influence of different water flow rates on these variables is evaluated using various computational models of the cavity receiver.

The determining criterion for selecting the optimal shape was to achieve the maximum temperature difference with the least pressure losses. The optimal shape identified through computational analysis was subsequently validated through experimental testing.

### 5.1 Group (A) (helically baffled path) results

The first group of models tested involved the helically baffled path, focusing on optimizing the key parameters of the helically baffled conical cavity receiver. The primary objective was to determine the optimal conical length, baffle pitch size, and inclination angle (upper conical diameter). A total of 27 models were tested, each differing in one or more of these parameters.

**First set of models (1-9):** The first set of models (Models 1-9) tested conical lengths equal to half of the aperture diameter ( $L = 0.5D$ ). The upper conical diameter ( $d$ ) and baffle pitch varied across these models. The parameters of these models are detailed in Table 7.

The results showed that models with a larger upper diameter (81 mm) performed slightly better in terms of temperature, with the highest recorded temperature being 299.154 K at a 2 L/min water flow rate. The inlet water temperature was consistently 297.15 K for all models. Model 9, which had the largest pitch size (20 mm), also exhibited the lowest pressure loss compared to the other models. Figure 14 illustrates the outlet temperature for Models 1-9, while Figure 15 shows the corresponding pressure losses.

**Second set of models (10-18):** The second set of models (Models 10-18) tested conical lengths equal to the aperture diameter ( $L = D$ ), while the other variables remained consistent with those in the first set. The dimensions for these models are provided in Table 8.

The results showed that Models 18 and 15 achieved the highest water outlet temperatures, with the maximum temperature recorded being 299.859 K at a 2 L/min water flow rate. Similarly to the first set, models with a pitch size of 20 mm exhibited lower pressure losses. Figure 16 and Figure 17 display the outlet temperatures and pressure losses for Models 10-18, respectively.

**Table 7.** Dimensions of models 1-9

Parameter	Model 1	Model 2	Model 3	Model 4	Model 5	Model 6	Model 7	Model 8	Model 9
Aperture size (D)	270 mm								
Conical length ( $L = 0.5D$ )	135 mm								
Upper diameter (d)	27 mm	54 mm	81 mm	27 mm	54 mm	81 mm	27 mm	54 mm	81 mm
Pitch size	10 mm	10 mm	10 mm	15 mm	15 mm	15 mm	20 mm	20 mm	20 mm

**Table 8.** Dimensions of models 10-18

Parameter	Model 10	Model 11	Model 12	Model 13	Model 14	Model 15	Model 16	Model 17	Model 18
Aperture size (D)	270 mm								
Conical length ( $L = D$ )	270 mm								
Upper diameter (d)	27 mm	54 mm	81 mm	27 mm	54 mm	81 mm	27 mm	54 mm	81 mm
Pitch size	10 mm	10 mm	10 mm	15 mm	15 mm	15 mm	20 mm	20 mm	20 mm

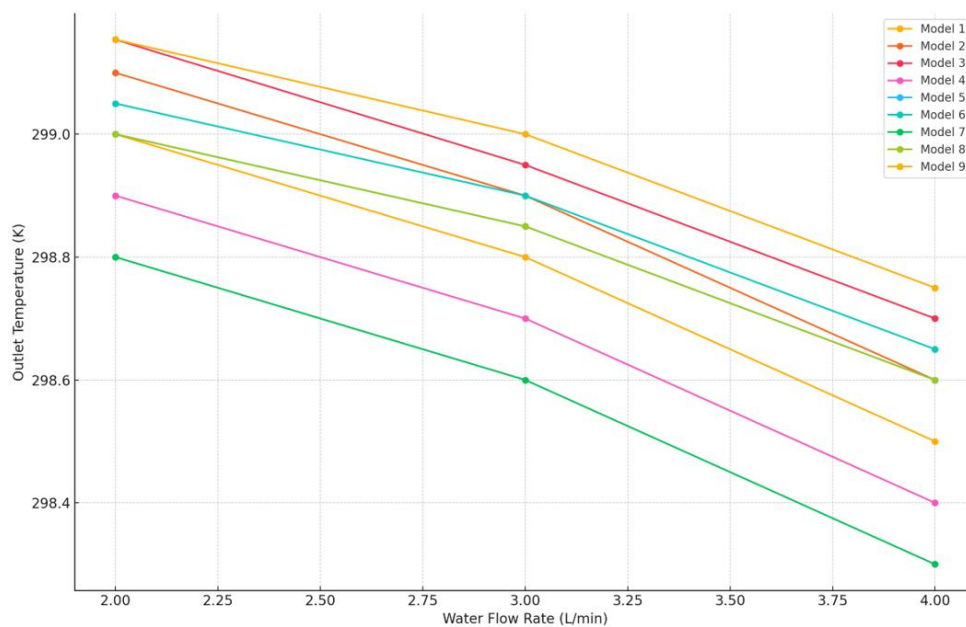


**Figure 14.** Outlet temperature vs water flow rate (helically baffled path models 1-9)

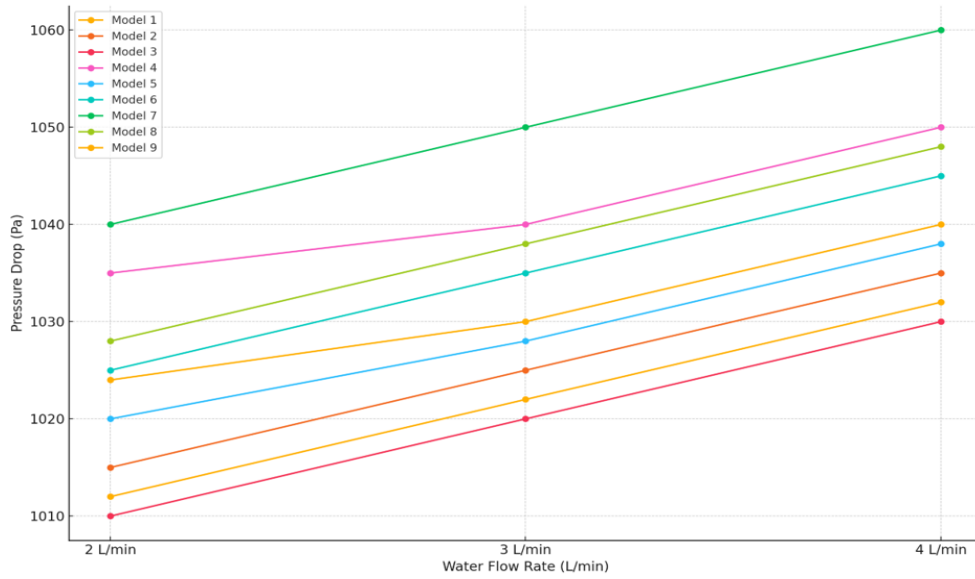


**Figure 15.** Pressure drop vs water flow rate (helically baffled path models 1-9)

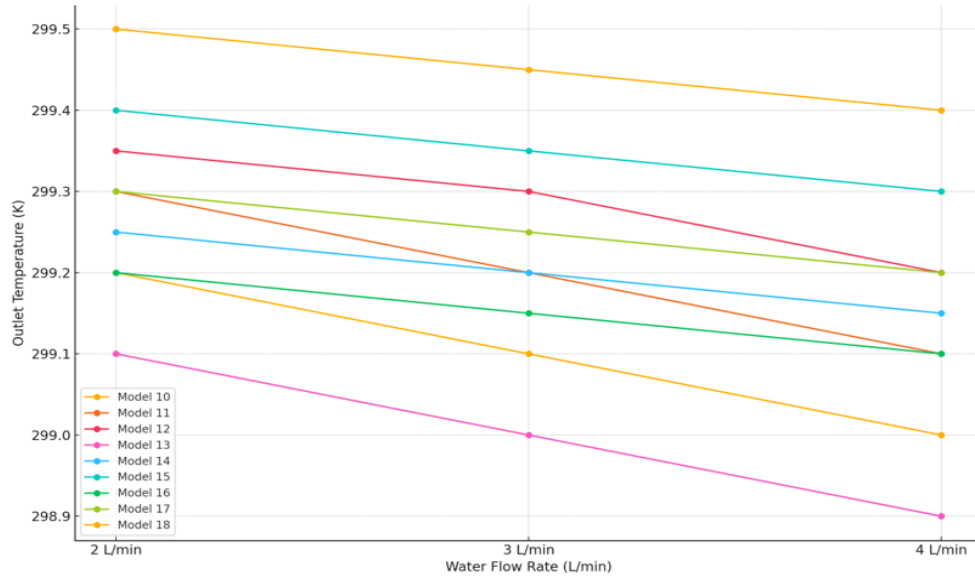


**Figure 16.** Outlet temperature vs water flow rate (helically baffled path models 10-18)

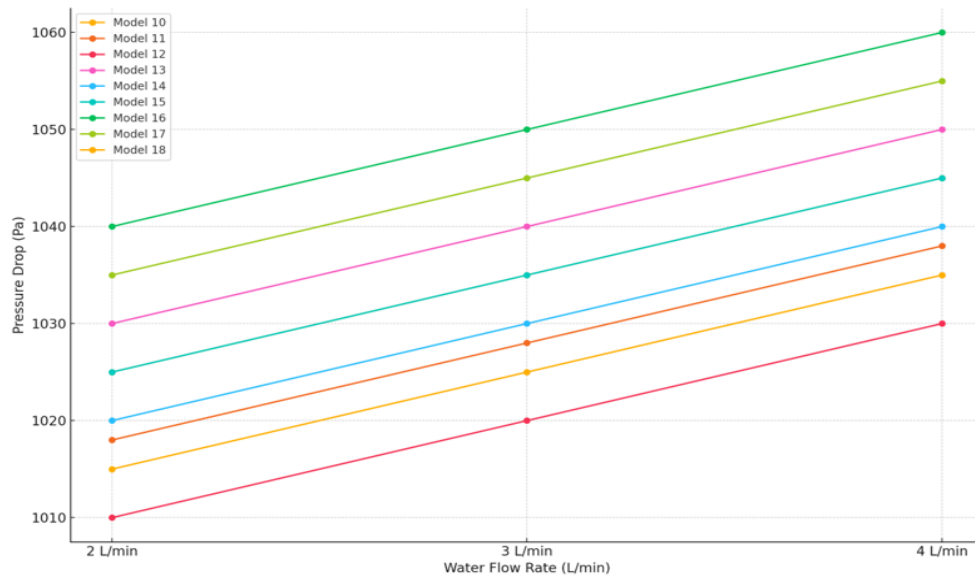


**Figure 17.** Pressure drop vs water flow rate (helically baffled path models 10-18)

**Third set of models (19-27):** The third set of models (Models 19-27) tested larger conical sizes, with conical lengths equal to 1.5 times the aperture diameter ( $L = 1.5D$ ). The results from these models are summarized in Table 9.

The CFD results from this set indicated that the highest outlet water temperature was achieved when the upper diameter was set to 81 mm Figure 18. However, the highest-

pressure losses were associated with models having a pitch size of 10 mm Figure 19.

Based on the results from the first 27 models, the optimal configuration was identified as having a conical length of  $1.5D$ , with an upper diameter of  $0.3D$  and a pitch size greater than 20 mm to minimize pressure losses.

**Table 9.** Dimensions of models 19-27

Parameter	Model 19	Model 20	Model 21	Model 22	Model 23	Model 24	Model 25	Model 26	Model 27
Aperture size (D)	270 mm								
Conical length ( $L = 1.5D$ )	405 mm								
Upper diameter (d)	27 mm	54 mm	81 mm	27 mm	54 mm	81 mm	27 mm	54 mm	81 mm
Pitch size	10 mm	10 mm	10 mm	15 mm	15 mm	15 mm	20 mm	20 mm	20 mm

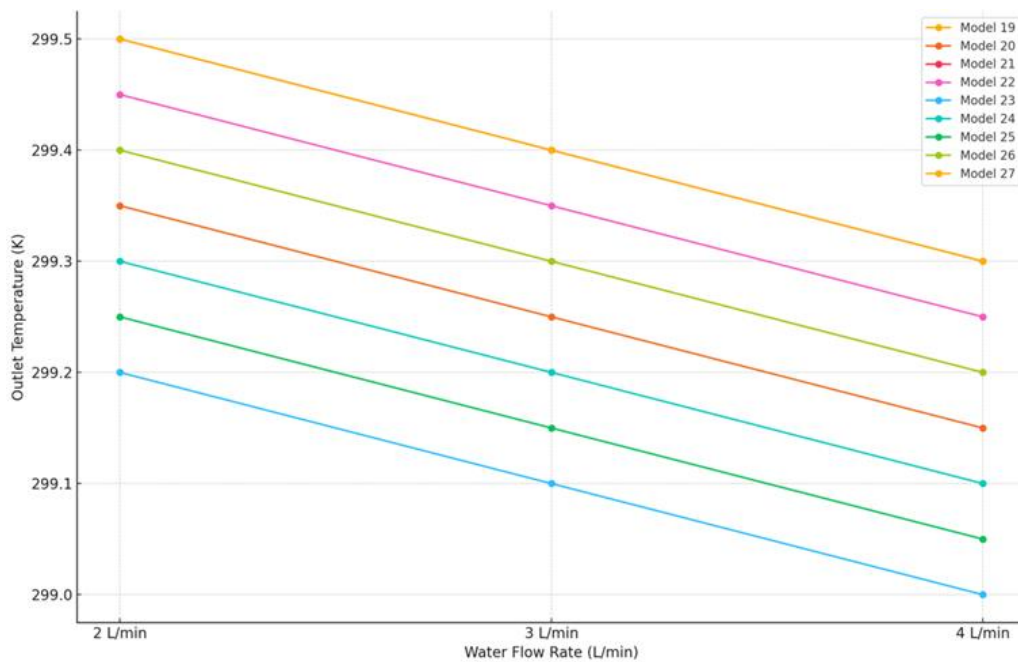


**Figure 18.** Outlet temperature vs water flow rate (helically baffled path models 19-27)

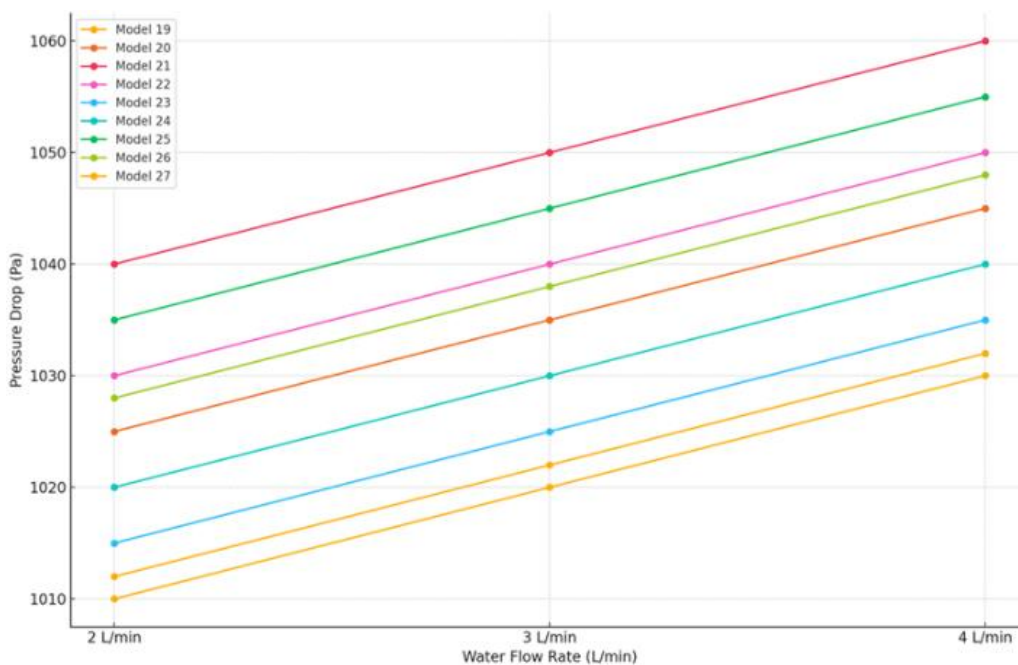


**Figure 19.** Pressure drop vs water flow rate (helically baffled path models 19-27)

## 5.2 Group (B) (helically baffled finned path) results

Following the identification of the optimal configuration in Group A, a new set of models featuring helically baffled finned paths was tested. The parameters for these models are detailed in Table 10.

The results from the helically baffled finned path models indicated a clear superiority over the previous helically baffled designs. The finned path configuration resulted in higher water outlet temperatures with lower pressure drops. Specifically, the maximum outlet water temperature achieved was 301.969 K at a water flow rate of 2 L/min, with a pressure drop of

145.835 Pa. This was recorded for the 3 mm finned path with a pitch size of 25 mm (Fin Model 1).

Interestingly, while the 6 mm finned path showed a similar outlet water temperature, it also exhibited a slightly higher pressure drop, indicating a trade-off between thermal performance and pressure loss. These results suggest that while increasing fin size can improve thermal efficiency, it may also increase pressure losses. The parameters and results are detailed in Figure 20 and Figure 21, which show the outlet temperature and pressure drop for the various finned path models.

**Table 10.** Dimensions of the helically baffled finned path models

Parameter	Fin Model 1	Fin Model 2	Fin Model 3	Fin Model 4	Fin Model 5	Fin Model 6	Fin Model 7	Fin Model 8	Fin Model 9
Aperture size (D)	270 mm								
Conical length (L = 1.5D)	405 mm								
Upper diameter (d = 0.3D)	81 mm								
Pitch size	25 mm	25 mm	25 mm	40 mm	40 mm	40 mm	60 mm	60 mm	60 mm
Fin size	3 mm	6 mm	9 mm	3 mm	6 mm	9 mm	3 mm	6 mm	9 mm

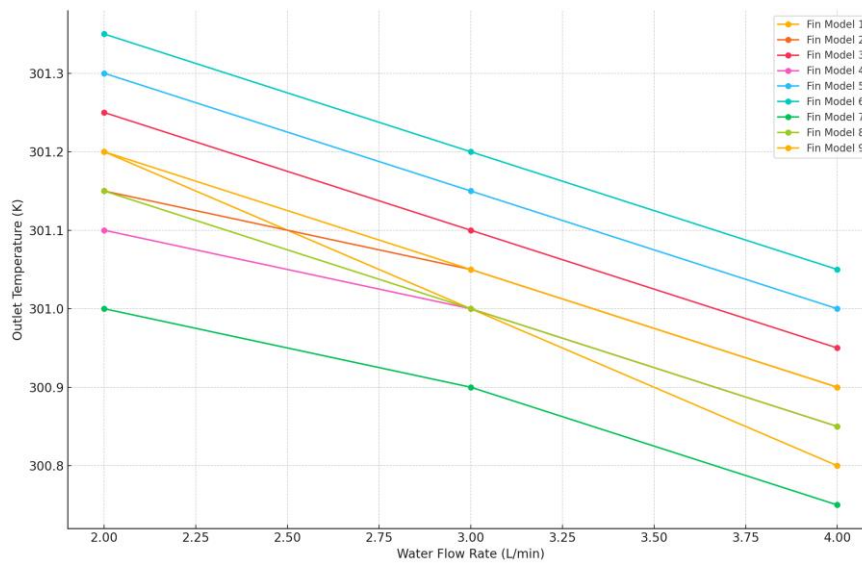


**Figure 20.** Outlet temperature vs water flow rate (helically baffled finned path models)

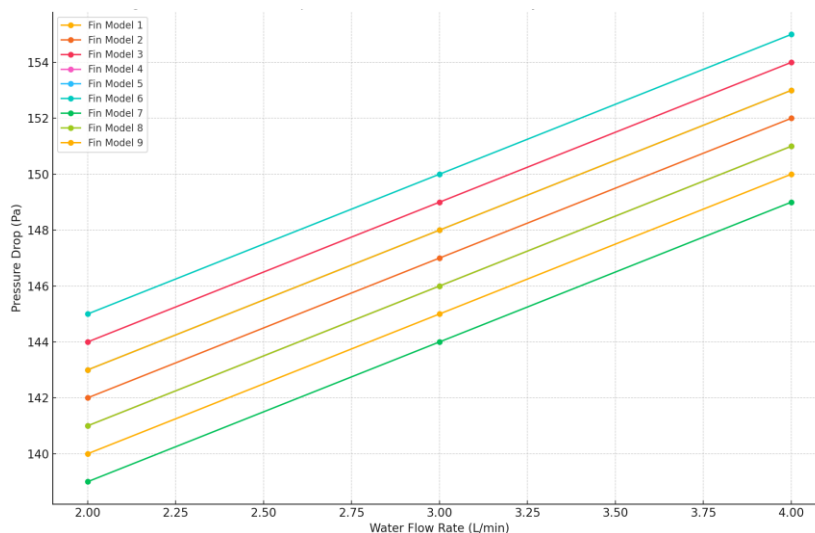


**Figure 21.** Pressure drop vs water flow rate (helically baffled finned path models)

### 5.3 Group (C) (multi-stage helically baffled finned path) results

Given the promising results from Group (B), a new set of models featuring multi-stage helically baffled finned paths was tested. This design combined different fin sizes to enhance fluid mixing within the receiver, potentially leading to improved thermal performance. The dimensions for the multi-stage finned path models are provided in Table 11.

The results from the multi-stage finned path models revealed that combining different fin sizes can indeed enhance the thermal performance. The best results were obtained with a pitch size of 60 mm, achieving a water outlet temperature of 301.748 K and a pressure drop of 169.555 Pa at a 2 L/min water flow rate. However, the model with a pitch size of 30 mm showed very close results, with an outlet temperature of 301.685 K and a pressure drop of 160.305 Pa at the same flow rate. These results are illustrated in Figure 22 and Figure 23.

**Table 11.** Dimensions of the multi-stage helically baffled finned path models

Parameter	Multi-Stage Model 1	Multi-Stage Model 2	Multi-Stage Model 3
Aperture size (D)	270 mm	270 mm	270 mm
Conical length ( $L = 1.5D$ )	405 mm	405 mm	405 mm
Upper diameter ( $d = 0.3D$ )	81 mm	81 mm	81 mm
Pitch size	30 mm	60 mm	90 mm
Fin size	3 mm and 6 mm combined	3 mm and 6 mm combined	3 mm and 6 mm combined

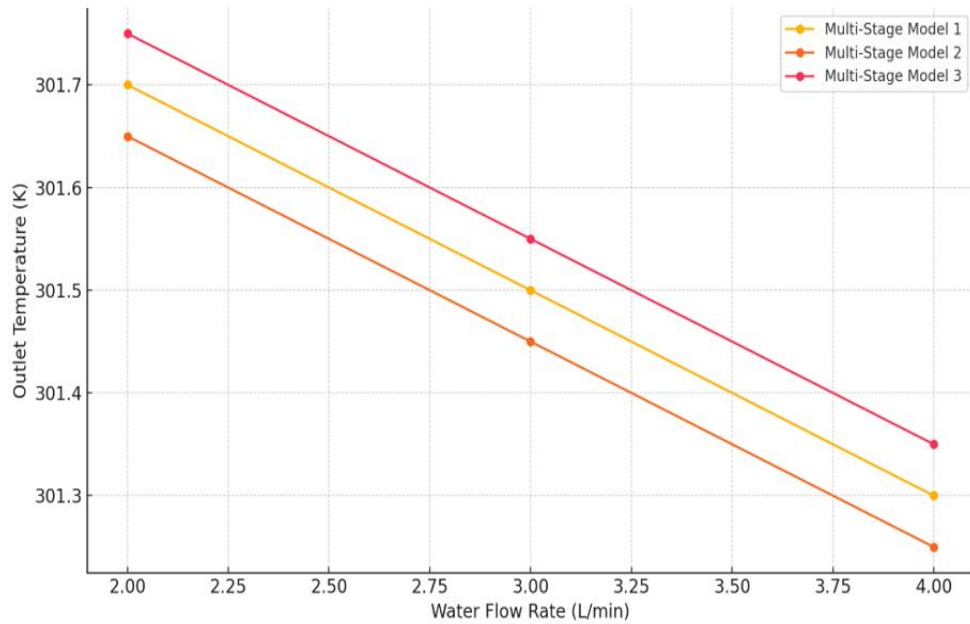


**Figure 22.** Outlet temperature vs water flow rate (multi-stage helically baffled finned path models)

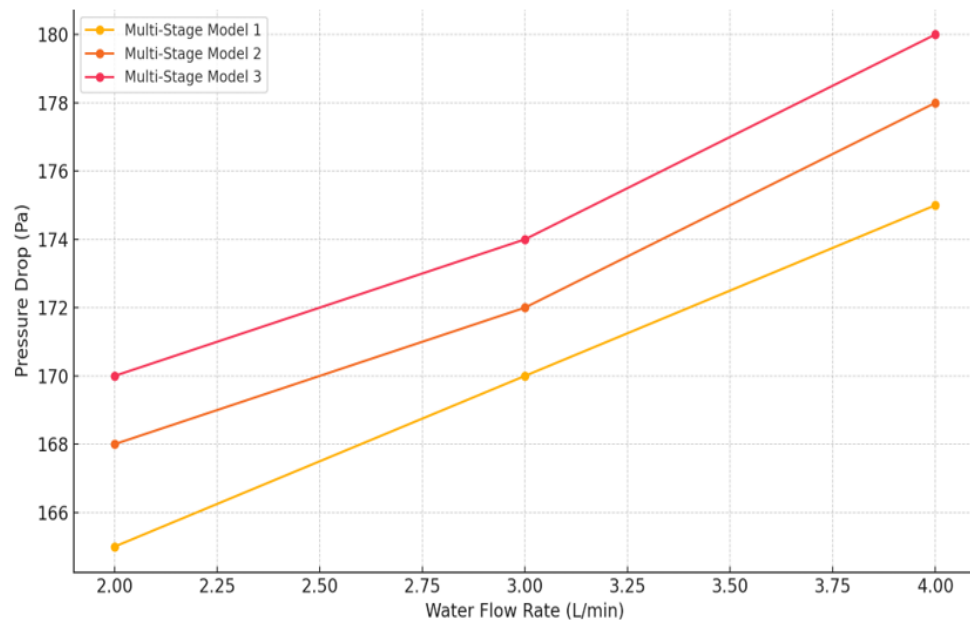


**Figure 23.** Pressure drop vs water flow rate (multi-stage helically baffled finned path models)

### 5.4 Experimental results

As previously mentioned, the optimal configuration identified from the CFD analysis was the helically baffled finned path with a 3 mm fin size and a 25 mm pitch size (Fin Model 1). This model was manufactured and tested experimentally to validate the CFD results.

The experimental results showed a strong correlation with

the CFD predictions. Figure 24 illustrates the thermal efficiency of the helically baffled finned conical cavity receiver throughout the day, while Figure 25 shows the relationship between temperature difference and solar irradiation. For comparison, a reference model with a circular receiver was also tested, and the results are displayed in Figure 26.

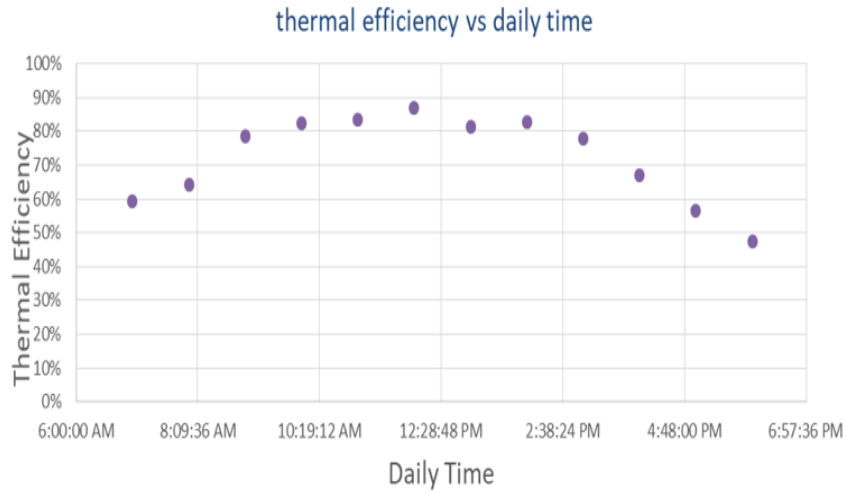


Figure 24. Helically baffled finned conical cavity receiver thermal efficiency vs daily time

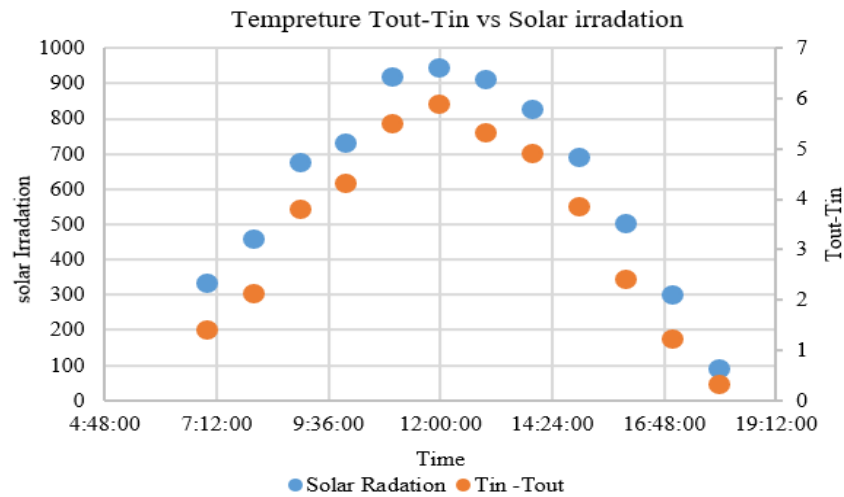


Figure 25. Helically baffled finned conical cavity receiver temperature difference vs solar irradiation

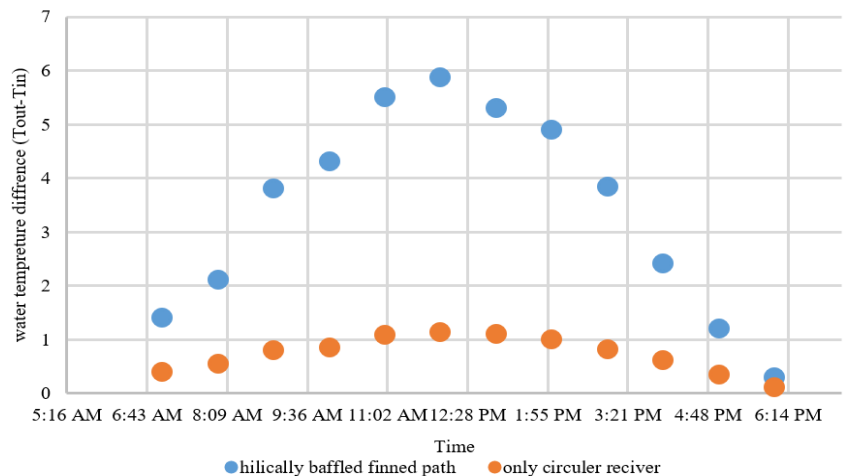
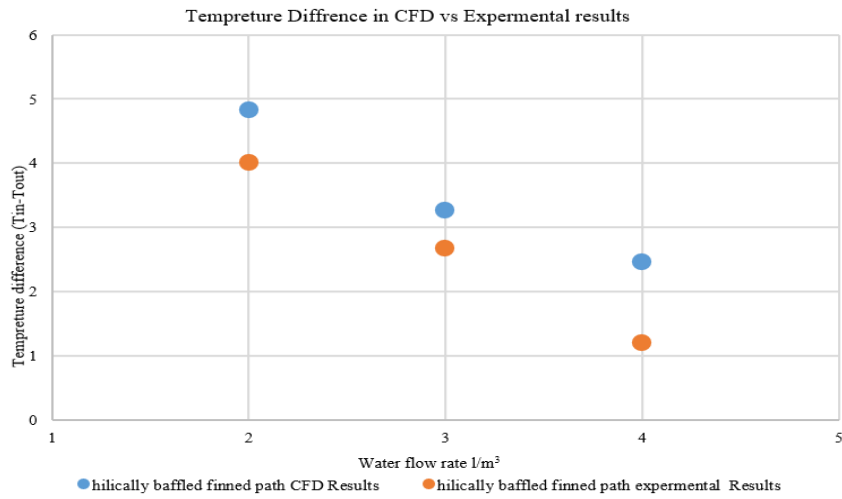
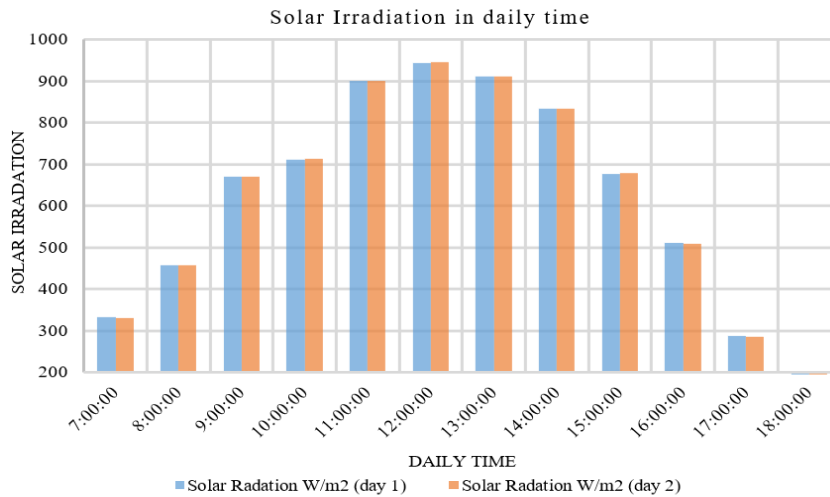


Figure 26. Temperature difference in helically baffled finned conical cavity receiver vs circular receiver CFD validation



**Figure 27.** CFD and experimental results in helically baffled finned conical cavity receiver



**Figure 28.** Solar irradiation in test daily time

To further validate the CFD results, a comparison was made between the CFD simulations and the experimental data. The validation was conducted by testing different water flow rates under nearly the same heat input (700 W). Additionally, the impact of varying solar input was also tested. The results are shown in Figure 27 and Figure 28.

This yields a good match between CFD predictions and experimental results and again testifies to the soundness of the design of the helically baffled finned path in countering common heat loss mechanisms like convective and radiative losses, which are difficult to manage in solar dish concentrators. This design gives further improvements in heat transfer performance that will not only elevate the overall thermal efficiency but also the long-term reliability and durability of the system by continuing to maintain optimal temperature gradients even for variable conditions in input solar.

In addition, the successful validation of these models opens up new avenues for better optimization of solar energy systems. Further studies might then target scaling up the helically baffled finned path design to larger applications or integrating it with other sources of renewable energy. The realization of optimized designs can translate solar dish concentrators into a more viable and penetrating industrial and residential energy source, which will be a crucial step in the global transition to cleaner sources of energy.

## 6. CONCLUSIONS

This study focused on determining the optimum design of a helically baffled conical cavity receiver used in a solar dish concentrator. The research divided the designs into three categories: Group A (helically baffled path), Group B (helically baffled finned path), and Group C (multi-stage helically baffled finned path). A total of 39 models were evaluated across the groups, and the findings were validated using CFD simulations and experimental testing. The key conclusions are as follows:

- **Group A:** The optimal design was achieved with a conical length 1.5 times the aperture diameter and an upper diameter of 0.3D. Model 27 in this group yielded the highest outlet water temperature of 300.304 K with a 2 L/min water flow rate and an inlet temperature of 297.15 K.
- **Pressure Drop in Group A:** The lowest pressure drop was observed in Model 9, with a value of 1024.21 Pa under the same flow rate.
- **Group B:** Models 1 and 4 demonstrated the best thermal performance, with Model 1 producing an outlet water temperature of 301.969 K and a pressure drop of 145 Pa at a flow rate of 2 L/min. Model 4 produced a similar outlet temperature of 301.938 K under the same conditions.

- **Group C:** This group achieved the highest outlet temperature of 301.748 K, with a pressure drop of 169.555 Pa under the same inlet temperature and flow rate.
- **Overall Performance:** The helically baffled finned path design (Group B) demonstrated superior thermal performance with minimal pressure drop compared to the other designs.
- **Experimental Validation:** The results from CFD simulations closely matched the experimental findings from the fabricated Model 1 of Group B, confirming the accuracy of the simulation predictions.

In conclusion, the helically baffled conical cavity receiver design showed excellent thermal performance, particularly in the helically baffled finned path configuration. These results suggest significant potential for further optimization and enhancements in future research.

## REFERENCES

- [1] Devabhaktuni, V., Alam, M., Depuru, S.S.S.R., Green II, R.C., Nims, D., Near, C. (2013). Solar energy: Trends and enabling technologies. *Renewable and Sustainable Energy Reviews*, 19: 555-564. <https://doi.org/10.1016/j.rser.2012.11.024>
- [2] Kadhim, S.A., Al-Ghezi, M.K., Shehab, W.Y. (2023). Optimum orientation of non-tracking solar applications in Baghdad city. *International Journal of Heat and Technology*, 41(1): 125-134. <https://doi.org/10.18280/ijht.410113>
- [3] Kadhim, S.A., Ibrahim, O.A.A.M. (2021). Improving the thermal efficiency of flat plate solar collector using nano-fluids as a working fluids: A review. *Iraqi Journal of Industrial Research*, 8(3): 49-60. <https://doi.org/10.53523/ijoirVol8I3ID86>
- [4] Abdul-Ghafoor, Q.J., Ali, F.A.M.A., Hasan, W.K., Hammoodi, K.A., Majdi, H.S. (2024). Enhancing thermal efficiency in solar water heaters using reflective mirrors. *International Journal of Design and Nature and Ecodynamics*, 19(1): 31-39. <https://doi.org/10.18280/ijdne.190104>
- [5] Khafaji, H.Q., Abdul Wahhab, H.A., Al-Maliki, W.A.K., Alobaid, F., Epple, B. (2022). Energy and exergy analysis for single slope passive solar still with different water depth located in Baghdad center. *Applied Sciences*, 12(17): 8561. <https://doi.org/10.3390/app12178561>
- [6] Hammoodi, K.A., Dhahad, H., Alawee, W., Omara, Z.M. (2024). Energy and exergy analysis of pyramid-type solar still coupled with magnetic and electrical effects by using matlab simulation. *Frontiers in Heat and Mass Transfer*, 22: 217-262. <http://doi.org/10.32604/fhmt.2024.047329>
- [7] Kadhim, S.A., Askar, A.H. (2018). Evaluation performance of a solar box cooker in Baghdad. *Journal of University of Babylon for Engineering Sciences*, 26(10): 208-216. <https://www.iasj.net/iasj/download/90703ead3f14c4b7>
- [8] Ibrahim, O.A.A.M., Kadhim, S.A., Ali, H.M. (2024). Enhancement the solar box cooker performance using steel fibers. *Heat Transfer*, 53(3): 1660-1684. <https://doi.org/10.1002/htj.23008>
- [9] Al-Ghezi, M.K., Abass, K.I., Salam, A.Q., Jawad, R.S., Kazem, H.A. (2021). The possibilities of using nano-CuO as coolants for PVT system: An experimental study. *Journal of Physics*, 1973(1): 012123. <https://doi.org/10.1088/1742-6596/1973/1/012123>
- [10] Ibrahim, O.A.A.M., Kadhim, S.A., Al-Ghezi, M.K.S. (2023). Photovoltaic panels cooling technologies: Comprehensive review. *Archives of Thermodynamics*, 44(4): 581-617. <http://doi.org/10.24425/ather.2023.149720>
- [11] Khelif, A.K., Al-Maliki, W.A.K., Abdul Wahhab, H.A., Alobaid, F., Epple, B., Abtan, A.A. (2023). Parabolic air collectors with an evacuated tube containing copper tube and spiral strip, and a new cavity receiver: Experimental performance analysis. *Sustainability*, 15(10): 7926. <https://doi.org/10.3390/su15107926>
- [12] Abdul-Ghafoor, Q.J., Abed, S.H., Kadhim, S.A., Al-Maliki, M.A. (2024). Experimental and numerical study of a linear Fresnel solar collector attached with dual axis tracking system. *Results in Engineering*, 23: 102543. <https://doi.org/10.1016/j.rineng.2024.102543>
- [13] Allouhi, H., Allouhi, A., Buker, M.S., Zafar, S., Jamil, A. (2022). Recent advances, challenges, and prospects in solar dish collectors: Designs, applications, and optimization frameworks. *Solar Energy Materials and Solar Cells*, 241: 111743. <https://doi.org/10.1016/j.solmat.2022.111743>
- [14] Li, X., Dai, Y.J., Wang, R.Z. (2015). Performance investigation on solar thermal conversion of a conical cavity receiver employing a beam-down solar tower concentrator. *Solar Energy*, 114: 134-151. <https://doi.org/10.1016/j.solener.2015.01.033>
- [15] Pavlovic, S., Loni, R., Bellos, E., Vasiljević, D., Najafi, G., Kasaeian, A. (2018). Comparative study of spiral and conical cavity receivers for a solar dish collector. *Energy Conversion and Management*, 178: 111-122. <https://doi.org/10.1016/j.enconman.2018.10.030>
- [16] Pavlovic, S., Daabo, A.M., Bellos, E., Stefanovic, V., Mahmoud, S., Al-Dadah, R.K. (2017). Experimental and numerical investigation on the optical and thermal performance of solar parabolic dish and corrugated spiral cavity receiver. *Journal of Cleaner Production*, 150: 75-92. <https://doi.org/10.1016/j.jclepro.2017.02.201>
- [17] Thirunavukkarasu, V., Sornanathan, M., Cheralathan, M. (2017). An experimental study on energy and exergy performance of a cavity receiver for solar parabolic dish concentrator. *International Journal of Exergy*, 23(2): 129-148. <https://doi.org/10.1504/IJEX.2017.085164>
- [18] Chu, S., Bai, F., Zhang, X., Yang, B., Cui, Z., Nie, F. (2018). Experimental study and thermal analysis of a tubular pressurized air receiver. *Renewable Energy*, 125: 413-424. <https://doi.org/10.1016/j.renene.2018.02.125>
- [19] Venkatachalam, T., Cheralathan, M. (2019). Effect of aspect ratio on thermal performance of cavity receiver for solar par dish concentrator: An experimental study. *Renewable Energy*, 139: 573-581. <https://doi.org/10.1016/j.renene.2019.02.102>
- [20] Bashir, M.A., Giovannelli, A. (2019). Design optimization of the phase change material integrated solar receiver: A numerical parametric study. *Applied Thermal Engineering*, 160: 114008. <https://doi.org/10.1016/j.applthermaleng.2019.114008>
- [21] Khalil, I., Pratt, Q., Spitzer, C., Codd, D. (2019). Modeling a thermoplate conical heat exchanger in a point focus solar thermal collector. *International Journal of Heat and Mass Transfer*, 130: 1-8. <https://doi.org/10.1016/j.ijheatmasstransfer.2018.10.041>

- [22] Hernandez, N., Riveros-Rosas, D., Venegas, E., Dorantes, R.J., Rojas-Morin, A., Jaramillo, O.A., Estrada, C.A. (2012). Conical receiver for a paraboloidal concentrator with large rim angle. *Solar Energy*, 86(4): 1053-1062. <https://doi.org/10.1016/j.solener.2011.09.008>
- [23] Xiao, H., Zhang, Y., You, C., Zou, C., Falcoz, Q. (2019). Effects of critical geometric parameters on the optical performance of a conical cavity receiver. *Frontiers in Energy*, 13: 673-683. <https://doi.org/10.1007/s11708-019-0630-2>
- [24] Zhang, Y., Xiao, H., Zou, C., Falcoz, Q., Neveu, P. (2020). Combined optics and heat transfer numerical model of a solar conical receiver with built-in helical pipe. *Energy*, 193: 116775. <https://doi.org/10.1016/j.energy.2019.116775>
- [25] Ansys Fluent. (2020). *Ansys Fluent Theory Guide*. ANSYS Inc., USA, 15317: 724-746.
- [26] Ibrahim, M.N.J., Hammoodi, K.A., Abdulsahib, A.D., Flayyih, M.A. (2022). Study of natural convection inside inclined nanofluid cavity with hot inner bodies (circular and ellipse cylinders). *International Journal of Heat and Technology*, 40(3): 699-705. <https://doi.org/10.18280/ijht.400306>
- [27] Abed, M.H., Al-Asadi, H.A., Oleiwi, A., Kadhim, S.A., Al-Yasiri, M., Alsayah, A.M., Nayyef, D.R. (2024). Improving building energy efficiency through ventilated hollow core slab systems. *Case Studies in Thermal Engineering*, 60: 104793. <https://doi.org/10.1016/j.csite.2024.104793>
- [28] Ansys. (2019). *Turbulence modeling. Introductory Fluent Training*, 34-35. <https://slideplayer.com/slide/14372519/>
- [29] Kadhim, S.A., Ibrahim, O.A.A.M. (2022). The effect of holes number in cylindrical samples on the forced convection heat flow. *International Journal of Mechanical Engineering and Robotics Research*, 11(6): 429-436. <http://doi.org/10.18178/ijmerr.11.6.429-436>
- [30] Nashee, S.R. (2024). Enhancement of heat transfer in nanofluid flow through elbows with varied cross-sections: A computational study. *International Journal of Heat and Technology*, 42(1): 311-319. <https://doi.org/10.18280/ijht.420133>
- [31] Fadhil, N.A., Al-Dabagh, A.M., and Hatem, F.F. (2023). Numerical investigation of heat transfer and pressure drop characteristics in a double pipe heat exchanger with corrugated tubes and rod baffles at various Reynolds numbers. *International Journal of Heat and Technology*, 41(3): 591-601. <https://doi.org/10.18280/ijht.410311>
- [32] Kadhim, S.A., Askar, A.H., Saleh, A.A.M. (2024). An enhancement of double pipe heat exchanger performance at a constant wall temperature using a nanofluid of iron oxide and refrigerant vapor. *Journal of Thermal Engineering*, 10(1): 78-87. <https://doi.org/10.18186/thermal.1429191>
- [33] Moshab, A.A., Aldulaimi, R.A.K.M. (2024). Thermal performance analysis of thermosyphon solar water heating system using overlapped and reverse flow. *International Journal of Heat and Technology*, 42(2): 593-602. <https://doi.org/10.18280/ijht.420226>
- [34] Ma, L., Yang, J., Liu, W., Zhang, X. (2014). Physical quantity synergy analysis and efficiency evaluation criterion of heat transfer enhancement. *International Journal of Thermal Sciences*, 80: 23-32. <https://doi.org/10.1016/j.ijthermalsci.2014.01.021>
- [35] Webb, R.L. (1981). Performance evaluation criteria for use of enhanced heat transfer surfaces in heat exchanger design. *International Journal of Heat and Mass Transfer*, 24(4): 715-726. [https://doi.org/10.1016/0017-9310\(81\)90015-6](https://doi.org/10.1016/0017-9310(81)90015-6)